PAPERS | AUGUST 01 2017

Zeeman effect experiment with high-resolution spectroscopy for advanced physics laboratory

Andrew S. Taylor; Alexander R. Hyde; Oleg V. Batishchev

Am. J. Phys. 85, 565–574 (2017)
https://doi.org/10.1119/1.4984809

Zeeman effect experiment with high-resolution spectroscopy for advanced physics laboratory

Andrew S. Taylor, Alexander R. Hyde, and Oleg V. Batishchev
Department of Physics, Northeastern University, Boston, Massachusetts 02115

(Received 20 September 2016; accepted 18 May 2017)

An experiment studying the physics underlying the Zeeman effect and the Paschen-Back effect is developed for an advanced physics laboratory. We have improved upon the standard Zeeman effect experiment by eliminating the Fabry-Perot etalon, so that virtually any emission line in the visible spectrum can be analyzed. The magnetic field is provided by neodymium magnets. Light emitted in the ∼1 T field is analyzed by a Czerny-Turner spectrograph equipped with medium-dispersion grating and small-pixel imaging CCD. A spectral resolution under 1 pm/pixel is achieved. The splitting of argon and helium lines is measured as a function of field strength. The proportionality of the splitting magnitude to the B-field strength and to λ^2 is demonstrated. The Bohr magneton is calculated and compared to the theoretical value. © *2017 American Association of Physics Teachers.*
[http://dx.doi.org/10.1119/1.4984809]

I. INTRODUCTION

In 1896, Pieter Zeeman observed a widening of the sodium D line in the presence of a magnetic field and found that the degeneracy of the energy levels in the atom had lifted.[1] He was later able to resolve the widening into three peaks.[2,3] This new phenomenon was first explained classically by Zeeman and Lorentz as a change in the precessional frequency of an electron in an atom.[4] In the years following his discovery of the "normal" Zeeman effect, triplet splitting was observed in other elements as well as "anomalous" splitting into four, six, or nine peaks.[5–7] The anomalous effect could not be explained until the advent of quantum theory. The discovery of electron spin[8,9] was a direct consequence of solving the problem of the anomalous splitting,[10–13] which led to the formation and subsequent validation of quantum mechanics.

Measurement of the Zeeman effect in atoms has continued to be an important tool for many active fields of research. The splitting of lines is used as a measure of impurity transport in magnetically confined fusion[14,15] as well as a method to measure the magnetic field strength.[16] Zeeman spectroscopy has been used to study the symmetry and crystal structure of doped GaAs,[17] a material useful in designing X-ray detectors,[18] and it is the only technique available to remotely measure the strength of a magnetic field in stellar or solar objects, for example, in sunspots[19] or rotating stars.[20–22] The splitting of molecular band peaks allows for the identification of the chemical composition of distant stars.[23] Numerical modeling of the Zeeman effect of atoms in a magnetic field is used to calculate hyperfine energy level changes.[24]

Despite its importance in spectroscopic measurements, the effect is difficult to observe due to the size of the perturbation to the energy level. Indeed, an external magnetic field $\mathbf{B}$ exerts a torque on the electron's magnetic dipole $\boldsymbol{\mu}$, and the change in energy of an atomic level from its non-perturbed energy is

$$\Delta E_B = -\boldsymbol{\mu}\cdot\mathbf{B} = -\mu_B g_L m_J B, \tag{1}$$

where $\mu_B \approx 5.79\times10^{-5}$ eV/T is the Bohr magneton, g_L is the Landé g-factor, and m_J is the projection of the total angular momentum $\mathbf{J}=\mathbf{L}+\mathbf{S}$ (orbital plus spin) in the direction of the magnetic field.

An electron dipole transition between two perturbed levels is governed by the selection rules: $\Delta m_J = 0, \pm1$. The energy lost due to a transition from upper level p to lower level q will be emitted as a photon of wavelength λ as

$$E_p - E_q = \frac{hc}{\lambda}. \tag{2}$$

A small change in energy E_p or E_q will produce a small change in wavelength,

$$\Delta E = \Delta\left(\frac{hc}{\lambda}\right) = -\frac{hc}{\lambda^2}\Delta\lambda, \tag{3}$$

and by equating Eqs. (1) and (3), the magnitude of the wavelength shift is found to be

$$\Delta\lambda = \frac{\mu_B g_L \Delta m_J}{hc}\lambda^2 B. \tag{4}$$

In the normal Zeeman effect, $\mathbf{S}=0$, $\mathbf{J}=\mathbf{L}$, and $g_L=1$ for every energy transition. The central peak remains at λ (since $\Delta m_J = 0$) and the two side peaks are shifted by

$$\Delta\lambda(\text{nm}) = \pm\frac{\mu_B}{hc}\lambda^2 B, \tag{5}$$

which, for practical settings, is in the 5–20 pm range.

For his research on the effects of magnetism on radiative phenomena, Zeeman was awarded the Nobel prize in 1902. Because of its historic importance to the formulation of quantum mechanics and its widespread application in physics research, experiments introducing the Zeeman effect have been widely used in physics laboratory curricula. Initially, such experiments use predominantly interferometers[25] or very-high-resolution spectrometers such as an Ebert spectrograph.[26] The detection was initially done by direct visual observations or with photographic plates or films. Detailed instructions are readily available from experimental physics textbooks.[27,28] The experimental technique has been enriched by the availability of photomultipliers and more recently by CCD cameras.[29]

A common laboratory approach[30,31] for the Zeeman effect utilizes a tunable Fabry-Perot interferometer and an iron-

core electromagnet. The experiment is assembled with a monatomic spectral source, such as Hg or Na, positioned between two poles of a water-cooled electromagnet. Emitted light is passed through a narrow-band filter and focused on the etalon through a collecting lens. The interference fringes are sent through a telescope to increase the size of the image, and projected onto a CCD imaging camera or viewing plate.

The effectiveness of the etalon for Zeeman spectroscopy greatly depends on the reflectivity of the mirrors, quantified as the idealized finesse $\mathcal{F}$ of the etalon

$$\mathcal{F} = \frac{2\pi\sqrt{R}}{1-R}, \tag{6}$$

where R is the reflectivity of the mirrors for the wavelength observed. The greater the reflectivity, the greater the finesse and the higher the resolution, which relates to the finesse as $\delta\lambda = \lambda^2/s\mathcal{F}$, where s is the spacing between the mirrors. If $\delta\lambda < \Delta\lambda$ from Eq. (5), the peaks can be resolved. As an example, an etalon with high reflectivity of $R \approx 0.9$ and mirror spacing $s = 5$–12 mm can resolve Zeeman splittings of 0.5–1.2 pm for a 600-nm line.

While this resolution is sufficient to resolve the Zeeman splitting of similar lines due to a magnetic field, there are a few limitations to this approach. A piezoelectric controller is required for μm spacing adjustments to maintain a mirror tilt less than 0.5 arcsec. The mirrors themselves must be processed with multiple layers of dielectric coatings for high reflectivity of the wavelengths of interest, and the required R is only available in a narrow spectral region. The etalon, then, cannot be used to study the Zeeman effect over the broad visible spectrum. High sensitivity to temperature fluctuations also diminishes the parallelism of the mirrors. In the IR region, this necessitates liquid-nitrogen-cooling for adequate results.[32]

To overcome these shortcomings, we propose to measure the Zeeman effect using a permanent magnet system, with variable B-field strength, and a medium-resolution spectrometer with a modern small-pixel-size CCD imaging camera. The spectrometer provides the resolution necessary to capture the Zeeman splitting and can be applied to virtually any line in the visible region. This approach is based on the high-resolution spectroscopic system that we have developed for diagnostics of Doppler and isotopic shifts of spectral lines in moving plasmas and gas discharges.[33,34]

II. INITIAL PROOF OF CONCEPT

The initial setup consisted of 50-W gas discharge Geissler spectral tubes and a 125 V model SP200 Spectrum Tube Power Supply made by Pasco Scientific.[35] The glass tubes are 26 cm long, composed of two chambers with electrodes connected by a 10-cm capillary cylinder. The cylinder has an inner gas-filled bore of diameter 1.85 mm and an outer diameter of 7.8 mm. The tubes are available with various monatomic and diatomic gases, and metal vapors. Monatomic gases are commonly used in Zeeman effect physics labs.[27–29,31]

The magnetic field was produced by two cylindrical neodymium (NdFeB) magnets with axial magnetization, grade N50, measuring 25.4 mm in both diameter and height.[36] Figure 1(a) shows the magnets attached to the power supply on either side of the tube. This arrangement produced a B-field of ~0.8 T at the center of the spectral tube, measured

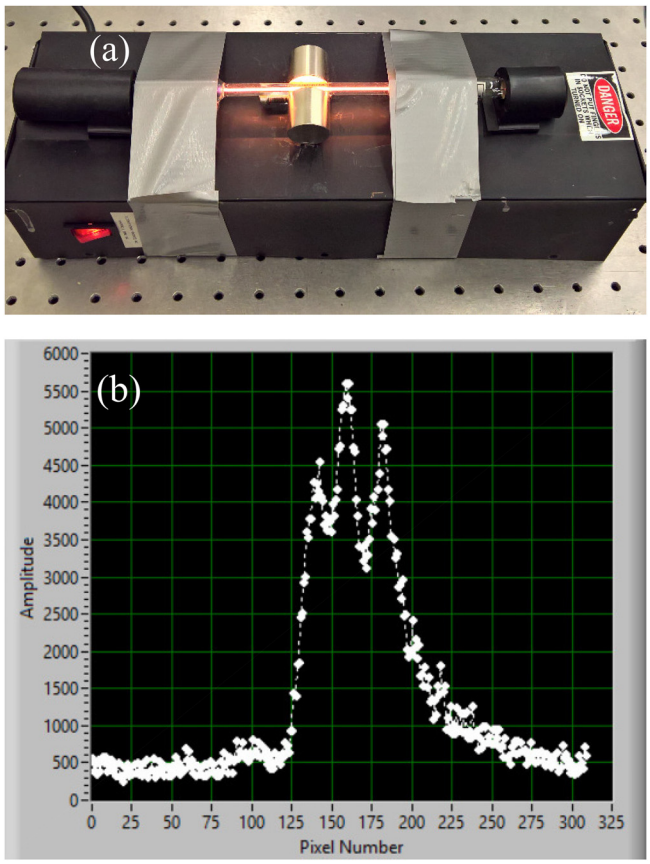

Fig. 1. (a) Initial experimental setup used to observe the Zeeman effect with minimal equipment. Two N50 grade neodymium magnets create a ~0.8-T field through a helium spectral tube, both attached to a Pasco Scientific Spectral Tube Power Supply. (b) Spectrum of the helium 706.519-nm line in a 0.8-T magnetic field split into three peaks via the Paschen-Back effect, as seen in the Labview VI to visualize the CCD image.

with a Hall-effect sensor. Initial tests were performed with hydrogen, because it produces a well-studied spectrum across the visible region with very bright lines. Unfortunately, the discharge was unstable in this configuration. Our second choice, helium, emitted a stable discharge.

One end of an optical fiber was pointed into the excited source while the other was attached to the entrance slit of a McPherson M216 spectrometer.[37] A 14-megapixel CCD camera[38] was placed at the exit focal plane and was controlled using a custom LabVIEW VI. The VI was programmed to view the entire 2D CCD image and to integrate a subset of pixels, creating a 1D plot of intensity vs pixel number. Figure 1(b) shows the He I 706.5-nm line taken with this initial configuration. The three peaks of the Zeeman splitting are clearly seen and spaced 20–21 pixels apart, corresponding to 19.6–20.3 nm and approximately equal to the $\Delta\lambda = 20$ nm calculated from Eq. (5). Thus, it was determined that a simple experiment could be created using just this equipment to study the Zeeman effect. Encouraged by these findings, we began to design a magnet holder with a variable and overall stronger B-field, and improved light collection capabilities.

III. EXPERIMENTAL APPARATUS

While a demonstration of the Zeeman effect can be completed with very simple parts as shown above, a more

elaborate setup is required for a versatile advanced laboratory experiment. The apparatus we propose consists of three main components: (A) the tunable magnet holder, (B) the light source and collection optics, and (C) the monochromator with small-pixel-size CCD camera.

A. Magnet holder for variable B-field

Figure 2 shows the custom magnet holder we designed and the frame built to secure it for experiments. The holder consists of two hollow arms and the main body, shown in Fig. 2(a), all milled out of aerospace-grade aluminum alloy 7075. The arms were machined specifically to hold two 50.8-mm cylindrical neodymium magnets with axial magnetization, grade N52. The stated remanence is ≈1.48 T, while the actual field at the center of each magnet face varies between 0.602 and 0.608 T.

The magnets are loaded with opposite polarity and secured with stainless steel set screws inside the arms. The grip of the screws is sufficient to oppose the pulling force of ∼1.5 kN when the magnets are brought close together. The outer surface of the arms are threaded for 1 mm per rotation and screw into either side of the body. The inside cavity of the body is threaded from either end, which meet in the center with a phase discontinuity. To account for this the magnets protrude from the edge of the arms. The protrusion also allows the field in the capillary of a spectral tube to be maximized without causing damage to the wider end chambers. Handles were added to the arms for controlled turning.

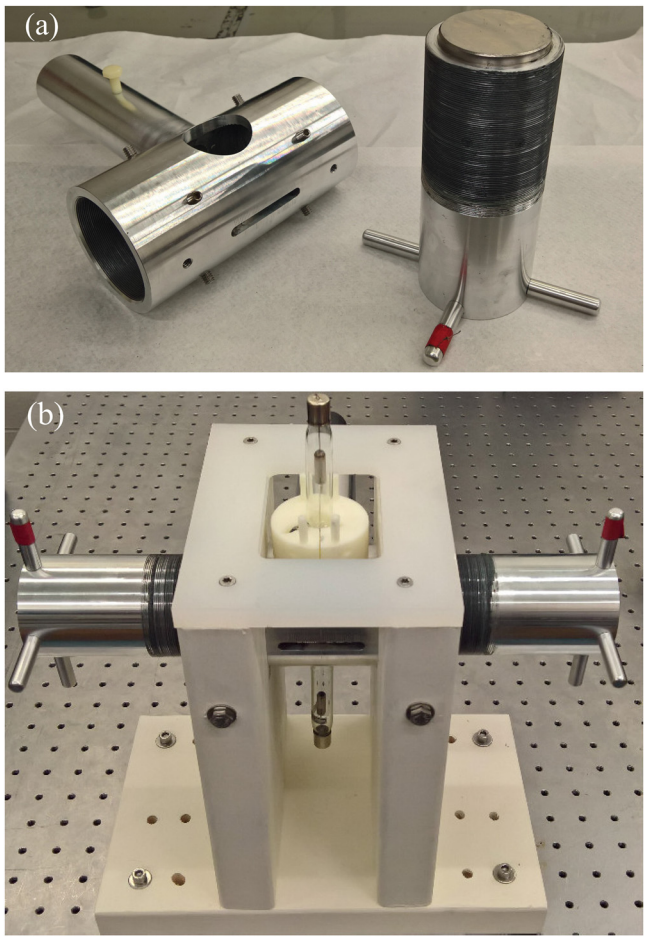

Fig. 2. The magnet holder for the Zeeman effect experiment. (a) Magnet holder body and an arm. The body is designed to house a spectral tube, two magnet arms, and collimating optics via the side extension. The magnet arms are loaded with the N52 magnets. (b) Magnet holder is secured in the solid frame. The body is between the two wooden walls and the side extension is sticking out the back. The arms are screwed into the body. The tube stopper is visible on the top.

The body has two 38 mm-diameter openings on the top and bottom, through which a spectral tube can be placed. A 44 mm-long slot was cut on the front side and notched with a scale of 1 mm markings; it provides access to view the light source and facilitates measurements of the spacing between magnets. Opposite to this opening, an aluminum side extension is welded to the body to house the collimation optics.

A sturdy frame was built around the holder and is shown in Fig. 2(b). The body was radially secured to the frame using four mounting bolts to provide the necessary support when rotating the magnet arms. The side frame pieces are attached to the base using stainless steel screws. A plastic top was added for further structural support. The frame was anchored to an optical Table with socket bolts. Lastly, prior to inserting the arms into the body, we lubricated the aluminum threads. We found that marine propeller grease was the most effective at reducing friction and erosion of the threads.

By changing the distance d between magnets, we can vary the B-field at the center of the spectral tube, facilitating a robust experiment that allows students to study the B dependence of the Zeeman splitting via Eq. (4). Figure 3(a) shows a plot of the B-field at the center of the holder as a function of d. The field was measured using a gaussmeter equipped with a Hall-effect sensor and was found to peak at 1.19 T with $d = 4$ mm. The field is also very uniform across the radial distance r from the center of the holder, shown in Fig. 3(b). Only absolute radial values are reported. The magnet holder provides a near-constant field in a 25 mm-diameter circle and allows for light collection from a large section of the source without significantly affecting the resultant Zeeman splitting.

B. Light source and focusing optics

We continued to use the Pasco spectral tubes as emission sources. We also designed and 3D-printed a custom stopper for the upper opening of the magnet holder, which secures a spectral tube in the center of the holder. The stopper consists of two half-moon pieces, with an 8 mm-diameter bore through the center and a countersink at the top to hold the tube's upper chamber. The pieces clamp around the tube and sit inside the top opening, shown in Fig. 2(b). To keep the stopper from falling through the holder, it was built with an overhang that sits flush with the curvature of the holder body. The stopper is made out of ABS plastic, which can withstand temperatures up to 105 °C. Note that the tubes can reach 90–95 °C during continuous operation, as measured with an infrared thermometer.

Using standard optical holders and lens tubes, we built double-lens collimators for collecting light and focusing it on the entrance slit of our M216 spectrometer. The front lens is a 75 mm-focal-length plano-convex lens, chosen so that the light collection cone is not blocked by the magnets when they are screwed in to $d = 8$ mm. The collimated beam is then focused onto an optical fiber using a 60 mm-focal-length lens, chosen to match the numerical aperture of 0.22 for a 450 μm-core Ocean Optics fiber. The collimator is placed into the side tube of the magnet holder. The symmetry of the holder, stoppers, and spectral tubes removes all but

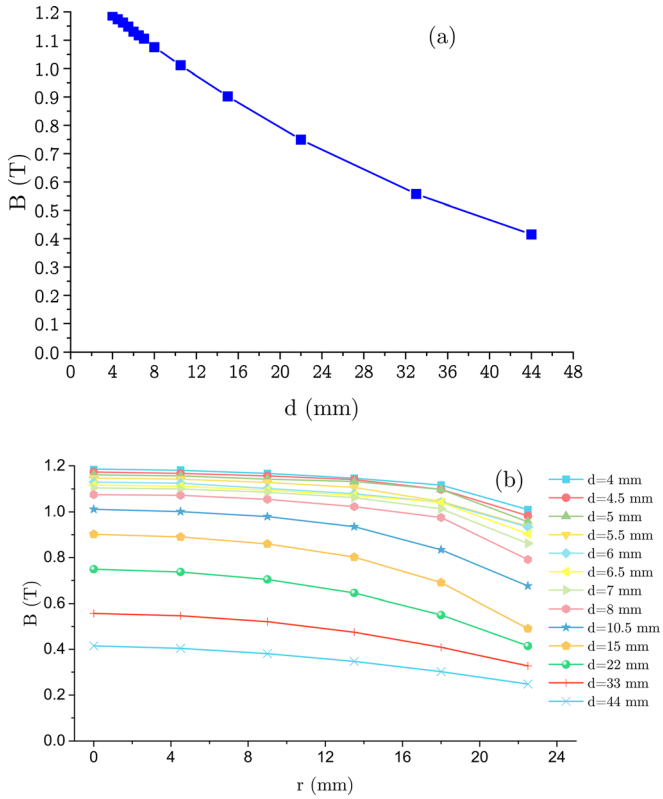

Fig. 3. (a) Magnetic field strength at $r = 0$ in the center of the magnet holder as a function of the magnet separation distance d, measured with a Hall-effect sensor. The maximum field measured is 1.17 T at $d = 4$ mm. (b) Magnetic field strength in the center of the magnet holder as a function of the radial displacement r from the axis of the holder, for different values of d.

one degree of freedom, which simplifies the focusing of the optics for the students. Once focused, the collimator is locked in place with two nylon screws on the top and bottom of the side tube.

C. Spectrometers and imaging sensor

Two spectrometers were employed. First, a hand-held UV–VIS Ocean Optics USB4000 spectrometer[39] was used to collect broad spectra from 194 to 909 nm, allowing us to verify that there is no emission <380 nm during spectral tube operation. Certain manufactured tubes brightly emit the helium 318 nm line, so UV safety must be taken into account if using similar tubes. The optical fiber from the collimator is plugged directly into the USB4000 and controlled by SpectraSuite software by Ocean Optics.[40] We can quickly re-position the collimator for maximum signal intensity.

Afterwards, the fiber is connected to the second two-lens collimator and focused on the 5-μm entrance slit of the high-resolution spectrometer, a McPherson Model M216 1 m-focal-length Czerny-Turner monochromator. It was designed as an asymmetric-optical-path spectrograph with coma-free spectral lines and is equipped with a 1200-g/mm grating, resulting in a spectral range of $\lambda_{min} \approx 200$ nm to $\lambda_{max} = 1000$ nm, and dispersion of 6.6 Å/mm. On the exit side, we removed the original 35 mm photographic film housing and installed a mount to position the AmScope MU1403 camera[38] at the focal plane. The camera has a 4096×3286 CCD array of square pixels with size $\Delta p = 1.4$ μm, giving a viewable wavelength range of 3.8×3.0 nm across.

IV. CHOICE OF GASES AND RESOLUTION CALIBRATION

While sodium would be necessary to recreate Zeeman's original experiment, compatible Na tubes are hard to obtain and operate. Helium and argon were ultimately chosen as the light sources used for the Zeeman effect experiment. The spectral tubes of these elements are readily available from many scientific suppliers. Both are monatomic gases, which eliminate the possibility of molecular bands in the spectra. Helium and argon are single-isotope elements with >99.6% purity,[41,42] unlike all other noble gases and many elements used in common spectral tubes such as mercury. This alleviates concerns regarding hyperfine isotopic shifts[34] in the spectra. Importantly, both have a rich spectrum of strong lines: helium across the entire visible region of 380–750 nm, argon across the upper-visible to near-infrared regions of 700–900 nm. Incidentally, the He I 706.5-nm and Ar I 706.7-nm lines nearly overlap, so the spectra can be stitched together into one VIS–NIR range. First, we identified suitable lines for the experiment using the Ocean Optics USB4000 spectrometer.

A. Helium

Figure 4(a) shows a typical spectrum produced by the helium tube, taken with the USB4000 spectrometer. Any line greater than 0.4 intensity can be viewed by the M216, with higher-count lines producing better signal-to-noise ratio (SNR). The strongest He I lines[41] usable for this experiment are shown in Table I. The triplet transitions (388 nm, 447 nm, 587 nm, and 706 nm) are composed of closely spaced emission lines, some of which can be identified as separate lines with the M216. These lines can then be used for self-calibration of the CCD and M216 per-pixel resolution.

Both the 587- and 706-nm lines have secondary peaks that are bright enough and spaced far enough apart to be resolved by the spectrometer. The 706 transition is shown in Fig. 5(a), which consists of two closely spaced lines at 706.517 nm and 706.521 nm (with an approximately 2:1 intensity ratio), interpreted as one main 706.519-nm line, and a separate 706.571-nm line. The separate line is hard to resolve due to the overall low intensity, but is still visible. Maximum peak location was determined by the maximum intensity pixel. The peaks are displaced by 58 pixels, yielding $\Delta r_p \approx 0.90$ pm/pixel.

B. Argon

Figure 4(b) shows the spectrum produced by the argon tube; it has strong VIS–NIR lines between 696 nm and 842 nm. The strongest Ar I lines used are: 696.54 nm, 750.39 nm, 751.46 nm, 763.51 nm, 810.37 nm, and 811.53 nm. Since all argon lines represent singlet transitions, a different method must be employed for calibration. Luckily, there are closely spaced lines that can be used. The tight and bright "doublets" of Ar I, 750/751 nm and 810/811 nm, are close enough to fit within the spectral range of the CCD array.

The 810/811 nm pair is shown in Fig. 5(b). The 811-nm line is the brighter of the two and displaced from 810 nm by 1356 pixels, yielding $\Delta r_p \approx 0.857$ pm/pixel. The increasing pixel resolution of the spectrometer at longer wavelengths, coupled with the λ^2 dependency in Eq. (4), shall result in greater magnitude of the Zeeman splitting.

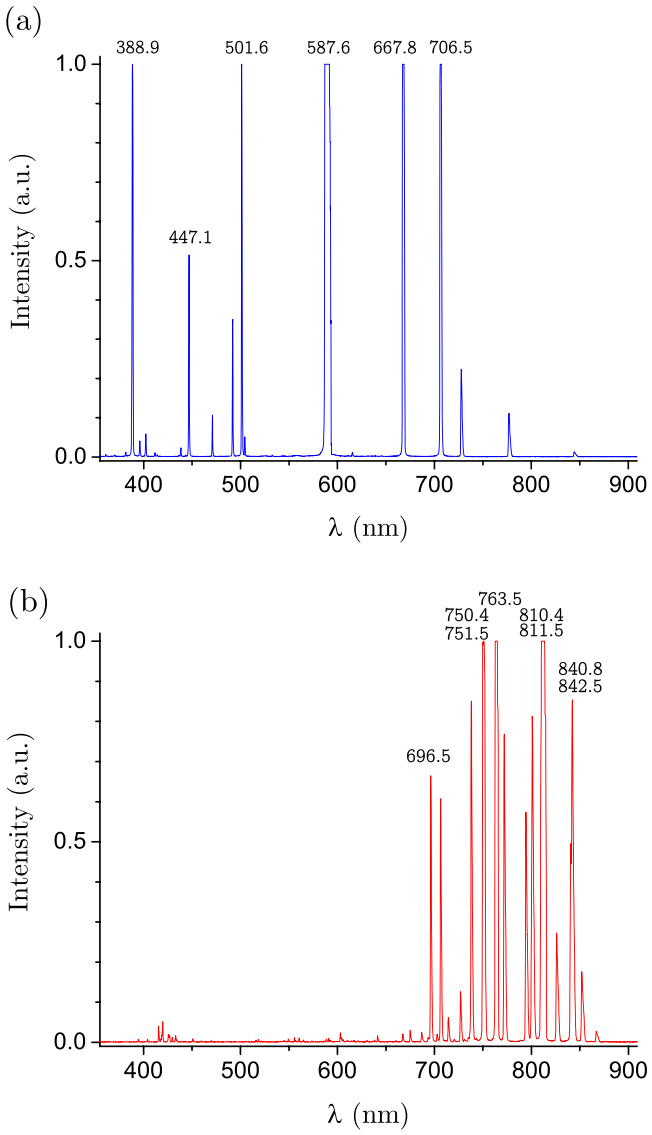

Fig. 4. (a) Helium spectrum obtained with the Ocean Optics USB4000 spectrometer for the Pasco spectral tube, with 10-ms exposure time and $B = 1$ T. (b) Argon spectrum obtained under the same conditions.

V. RESULTS FOR HELIUM

A. Paschen-Back effect

While increasing the B-field does increase the wavelength separation of the Zeeman effect peaks, it also changes the pattern of lines that can be observed. Friedrich Paschen and Ernst Back found that the anomalous Zeeman effect changed into the characteristic normal splitting when the magnetic field is increased above a certain limit.[43] In the Paschen-Back effect, the energy perturbation ΔE_B from the magnetic field is on the order of the perturbation from the spin-orbit coupling, so that the total angular momentum is decoupled into its respective orbital and spin components. In the strong-field limit Eq. (1) becomes

$$\Delta E_B = -\mu_B(m_L + 2m_S)B, \tag{7}$$

where m_L and m_S are the projection of **L** and **S**, respectively, along the direction of **B**. A dipole transition obeys the selection rules: $\Delta m_L = 0, \pm 1$ and $\Delta m_S = 0$. The latter is required to preserve the polarization of a line.[4] Accordingly, the change in wavelength in the Paschen-Back limit is given by

$$\Delta\lambda(\text{nm}) \simeq 4.665 \times 10^{-8}\lambda^2 B, \tag{8}$$

with values substituted for constants, B in Tesla, and λ in nm. This result is equivalent to the normal Zeeman effect splitting of Eq. (5).

Due to the relatively small internal field in a helium atom, the transition between Zeeman splitting and the Paschen-Back approximation occurs in the 0.1–0.4 T region.[44] In higher fields, the complex Zeeman patterns should converge into triplets. With this in mind, we measured the Zeeman effect for each of the six brightest helium lines in Fig. 4(a). The spectral tube was secured in the center of the holder using the stopper, and the magnet arms were screwed in until $d = 8$ mm, resulting in a starting $B = 1.07$ T field in the center of the tube.

The normal Zeeman effect dependence on magnetic field strength and wavelength are shown in Fig. 6. With wavelength held constant, an increasing B-field increases the triplet splitting. This is demonstrated in Fig. 6(a) for the He I 706-nm line. At $B = 1.07$ T (solid line), the peaks are spaced ~27 pixels apart, while at $B = 0.8$ T (dashed line) the peaks are spaced apart by ~20 pixels. Figure 6(b) shows the He I 447-nm line at $B = 1.07$ T. Here, the peaks are spaced ~10 pixels apart. This demonstrates that in our experimental setup, both types of dependencies on B and λ can be investigated.

B. Measurement of the Bohr magneton

Since the magnetic field strength can be easily varied inside the magnet holder without disrupting the optical collection, we devised an experiment to measure the Bohr magneton. The linear dependence of B allows for a simple calculation of μ_B and comparison with the theoretical value of $\approx 5.79 \times 10^{-5}$ eV/T.

Table I. Prominent VIS and NIR spectral lines for helium and argon transitions. The average pixel spacing between peaks at $B = 1.07$ T is recorded along with the corresponding $\Delta\lambda$ Zeeman split value. From the linear regression analysis of lines > 400 nm, a value for μ_B and uncertainty is calculated.

Element	Transition	λ (nm)	Average pixel spacing	$\Delta\lambda$ (pm)	μ_B ($\times 10^{-5}$ eV/T)	$\delta\mu_B$ ($\times 10^{-5}$ eV/T)
He I	2^3S–3^3P	388.9	7.2	7.6	—	—
He I	2^3P–4^3D	447.1	9.7	10.0	7.88	2.5
He I	2^1S–3^1P	501.6	12.5	12.4	7.74	2.0
He I	2^3P–3^3D	587.6	17.6	17.0	6.10	0.72
He I	2^1P–3^1D	667.8	22.8	21.0	5.44	0.74
He I	2^3P–3^3S	706.5	27	24.2	5.25	0.54
Ar I	$^2[3/2]2$–$^2[5/2]3$	811.5	41.5	35.6	5.56	0.19

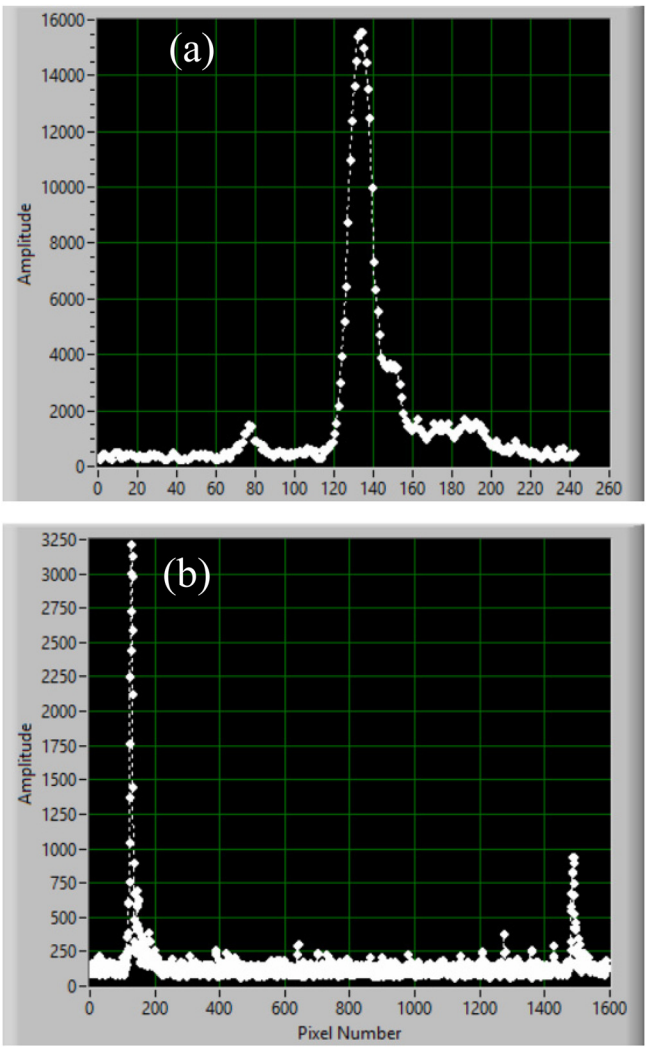

Fig. 5. Intensity vs pixel number at $B = 0$ used for per-pixel resolution calculations for helium and argon, displayed in the LabVIEW VI. Peak position was determined as maximum intensity pixel. (a) He I 706-nm line. The 706.519-nm strong peak and 706.571-nm peak to the left are spaced 0.052 nm and 58 pixels apart, yielding $\Delta r = 0.90$ pm/pixel resolution. (b) Ar I 810/811-nm "doublet." The weaker 810.37-nm peak and stronger 811.53-nm lines are spaced 1.1618 nm and 1356 pixels apart, yielding $\Delta r = 0.857$ pm/pixel resolution.

For each bright wavelength, we collected five spectral data sets at each of six different values of B. We unscrewed the magnet arms in whole number rotations for each B-field value based on the data in Fig. 3(a), so that field strengths of 1.07, 0.9, 0.8, 0.7, 0.6, and 0.5 T corresponded to magnet separations of $d = 8$, 14, 18, 22, 26, and 34 mm, respectively. As a check, the field was measured through the bottom hole or the side slot of the holder. This introduced experimental uncertainty in the B-field value, as the field could not be measured directly in the center of the magnets with the spectral tube suspended there.

Using the collected data, we found the spacing between the five left and five right peaks for each data set, again determined by maximum intensity. We averaged the ten spacings and calculated the standard deviation to quantify the uncertainties. The average spacing was converted into $\Delta\lambda$. We graphed $\Delta\lambda$ vs B and calculated a line of best fit using linear regression. The slope and y-intercept uncertainty were found using the Northeastern University Introductory Physics Laboratory (IPL) Straight-Line Fit website.[45]

Figure 7 shows plots of $\Delta\lambda$ vs B for the He I 587.6-nm and He I 667.1-nm lines. Setting the slope equal to $\Delta\lambda/B$ in Eq. (8), we calculated μ_B for each. This regression analysis has been done for the He I 447-nm, 501-nm, and 706-nm lines as well, with results shown in Table I. In our apparatus, wavelengths > 400 nm can be used to study the linear B-field dependency of the Zeeman effect and calculate a value for μ_B. The calculated value agrees with the known value, and the y-intercept crosses the origin, within error for each wavelength.

C. Analysis of λ^2 dependence

Because the spectrometer can resolve the splitting for practically any line in the visible spectrum, we can also use our experiment to demonstrate the linear dependence of $\Delta\lambda$ on λ^2 in Eq. (4). This is a unique feature of our system, as this analysis cannot be performed using a Fabry-Perot etalon. The etalon does not have the necessary finesse to resolve the Zeeman splitting over a broad spectral range. Using the

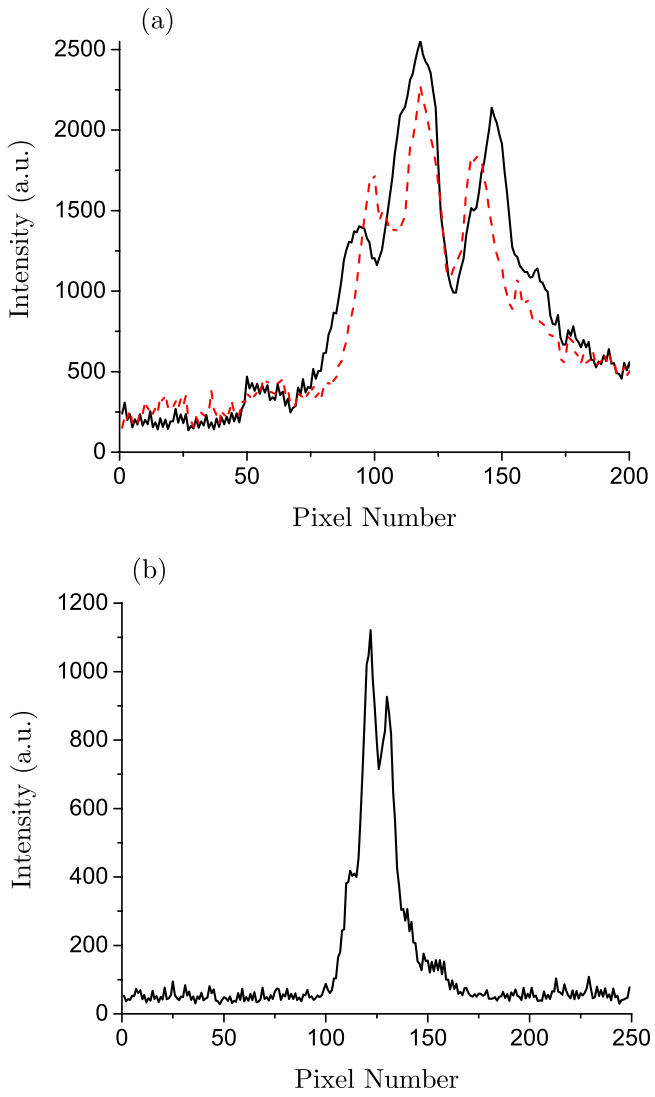

Fig. 6. Magnetic field and wavelength dependencies on the Zeeman effect. (a) Intensity vs pixel number showing B-field variation in triplet splitting of He I 706-nm line for $B = 1.07$ T (solid) and $B = 0.8$ T (dashed). The pixel spacing decreases with B. (b) Intensity vs pixel number of He I 447-nm line at $B = 1.07$ T. Compared to the 706-nm line, the 447-nm line has much smaller triplet splitting for the same field strength, showing wavelength dependence.

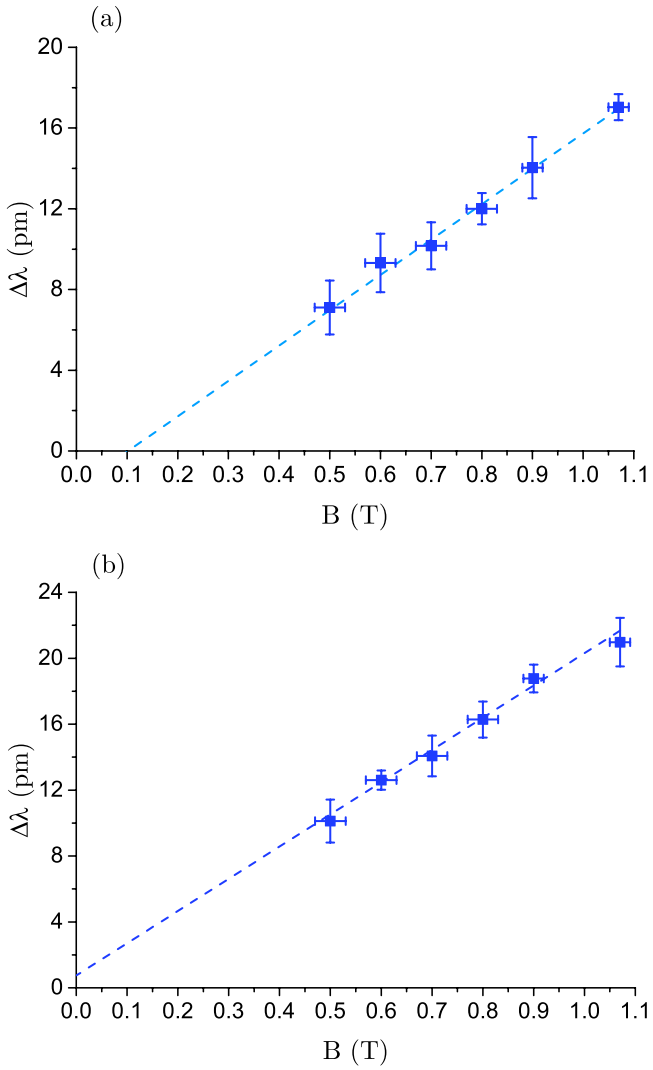

Fig. 7. Linearity of the triplet splitting in the Paschen-Back effect as a function of B-field. (a) The He I 587-nm line gives a Bohr magneton value of $(6.10\pm0.72)\times10^{-5}$ eV/T using the IPL Calculator (Ref. 45). (b) The He I 667 nm calculated Bohr magneton value is $(5.44\pm0.74)\times10^{-5}$ eV/T.

$B \lesssim 1.07$-T data for each of the six bright lines in helium, we plotted $\Delta\lambda$ vs λ^2 in Fig. 8. In order to demonstrate that the relationship is consistent with Eq. (8) as expected, we once again used regression analysis to calculate μ_B. The resulting value is $5.69\pm0.19\times10^{-5}$ eV/T, which agrees with the expected value within error. We believe this is a better method for calculating μ_B than the B-field dependency. The magnet spacing d is kept constant, reducing the uncertainty from rotating the arms, and the $B = 1.07$-T data have smaller $\Delta\lambda$ uncertainty due to more defined peaks than lower-field strengths.

D. Resolution limit and sources of errors

The resolution limit of the M216 spectrometer for the Zeeman effect occurs around 400 nm. The splitting for the 388-nm wavelength is too small to completely split into three peaks with this system. The line shows a definite second peak on the lower wavelength side of the image with a spacing of 8 pixels, and an unresolved bump on the higher wavelength side with a spacing of ~7 pixels. From this, the minimum practical resolution can be estimated as 7–8 pixels. Because the splitting could not be measured for $B < 1.07$ T, no value for μ_B is recorded in Table I. But the 388-nm line can be used to demonstrate Zeeman's original finding that the line widens in the magnetic field.[1] When it is measured at $B = 0$, the line is three times thinner than in the 1-T field.

Other systematic errors can be identified by analyzing the He I 706-nm spectra in Fig. 6(a). First, wavelengths too closely spaced to be resolved by the apparatus must be interpreted as a single wavelength. Also, the spectrometer distorts line shapes, in particular on the lower wavelength side. The $B = 0$ line in Fig. 5(a) has a small step, which is still visible in the two $B > 0$ cases. The triplets themselves are asymmetric, with less intensity on the upper wavelength side and a long attenuated "tail" on the lower side. In addition, the CCD has extraneous frozen pixels that manifest themselves as false features in the spectra. There are associated statistical fluctuations as well in reproducing the position of the spectral lines for multiple data sets, which is why we took an average of the five trials.

VI. RESULTS FOR ARGON

A. Zeeman effect in argon

To study the Zeeman effect in longer wavelengths, we used an argon spectral tube and continued probing beyond

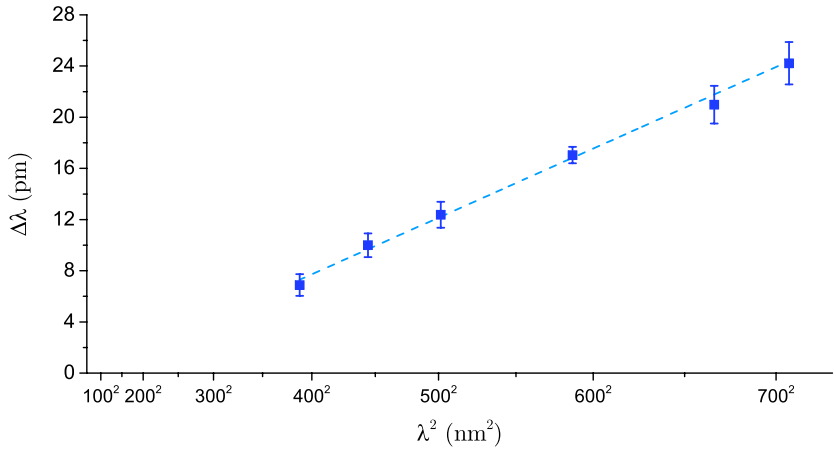

Fig. 8. Linearity of the Zeeman splitting due to the Paschen-Back effect as a function of λ^2. All six bright He I lines measured with $B = 1.07$ T are used. The Bohr magneton value calculated with the slope is $(5.56\pm0.19)\times10^{-5}$ eV/T.

706 nm. Figure 9 shows the spectrum at $B = 1.07$ T and results for the Ar I 811-nm line. In Fig. 5(b), the transition is split into three peaks according to Eq. (5) and is spaced 42 and 40 pixels apart. Figure 9(b) shows the B-field dependence of $\Delta\lambda$ measured for six magnetic field strengths, which has the same width proportionality factor in argon as it did in helium. Using the value of the slope, we calculated μ_B to be $5.61 \pm 0.58 \times 10^{-5}$ eV/T. Once again the relative error is $<10\%$ and the calculated value matches the theoretical within uncertainty.

B. Anomalous Zeeman effect

As it turns out, there are bright emission lines beyond the 909-nm limit of the USB4000 spectrometer. For instance, strong Ar I 912.3-nm and 965.8-nm lines are practically viewable in the M216 spectrometer range. However, the quantum efficiency of the MU1403 camera in the NIR range was not high enough to observe the 965-nm line. The 912-nm line, on the other hand, was observed successfully. To students' surprise, it splits into an anomalous sextet pattern,[46] as shown in Fig. 10. While the background noise signal is larger compared to VIS lines, six approximately equally spaced peaks are clearly defined. Other lines in argon could be used to demonstrate the anomalous Zeeman effect as well, which may allow students to calculate g_L along with μ_B for anomalous transitions.

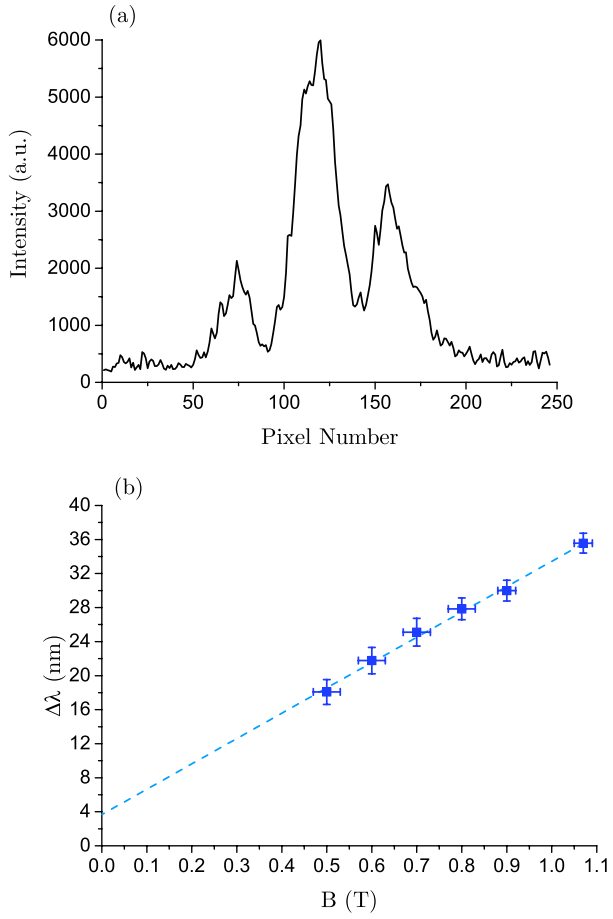

Fig. 9. Ar I 811.5-nm Paschen-Back measurements and calculations. (a) Intensity vs pixel number at $B = 1.07$ T. The average spacing between peaks is 41.5 pixels, resulting in $\Delta\lambda \approx 0.036$ nm. (b) Linearity of the triplet splitting as a function of B-field. The Bohr magneton value calculated from the slope is $(5.61 \pm 0.58) \times 10^{-5}$ eV/T.

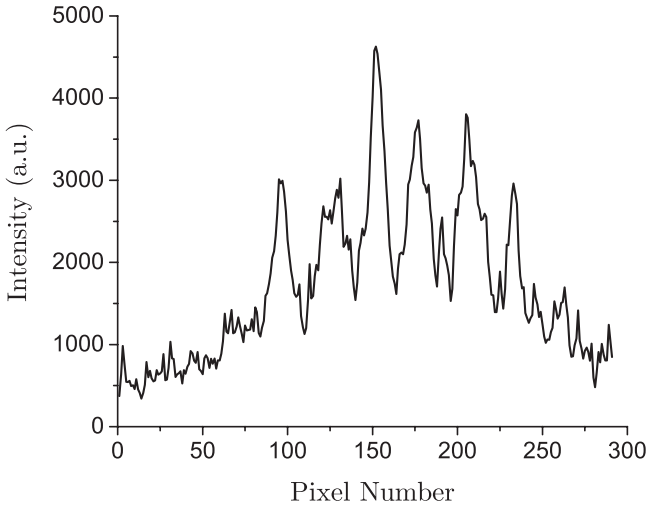

Fig. 10. Intensity vs pixel number of Ar I 912-nm line at $B = 1.07$ T, split into an anomalous sextet pattern. The strong line appears weak with a large background noise due to poor quantum efficiency of the CCD in IR.

VII. POSSIBLE IMPROVEMENTS AND CONSTRAINTS

The current setup can be modified by improving magnetic field strength, image sensor sensitivity, or wavelength range. The current magnets have an operational temperature of 80 °C, which is close to the spectral tube temperature of 90–95 °C that is achieved during continuous use. Using other rare-earth magnets with a higher Curie point would decrease the possibility of inadvertent demagnetization but would also likely decrease the B-field, as these typically have a lower remanence than the N52-grade NdFeB magnets. In principle, the field strength could be increased by approximately 20% by using larger magnets, but this would elevate safety concerns over possible injuries if the holder broke and the magnets came together.

Spectral resolution could be increased with a different grating or longer spectrograph. The 1200-g/mm grating in the M216 could be switched out for a higher 1800-g/mm grating. This change would increase resolution by 50% and would allow one to resolve all three peaks of the He I 388-nm Zeeman splitting. For instance, using a high-resolution 75-cm spectrometer[33] equipped with 3600-g/mm grating would more than double the current spectral resolution of the He I 388-nm line.

However, the increase in resolution would come at the cost of a smaller range of observable wavelengths. For example, the M216 with a 1200-g/mm grating allows for a maximum viewable wavelength of $\lambda_{\max} = 1000$ nm, while equipping it with a 2400-g/mm grating would decrease it to $\lambda'_{\max} = 500$ nm. The decrease in $\lambda_{\max}$ would remove the possibility of measuring any Ar I lines and all but the 388-nm and 447-nm He I lines. This would eliminate the unique ability to analyze the λ^2 dependency as demonstrated in Fig. 8.

It is easy to show that switching to a higher grating does not increase the maximum achievable pixel separation for Zeeman splitting, but rather does the exact opposite. If n is the ratio of the higher groove density to lower, the higher

groove density will improve the per-pixel resolution by $\Delta r'_p = \Delta r_p/n$ but will decrease proportionally the maximum viewable wavelength: $\lambda'_{\max} = \lambda_{\max}/n$. The new maximum Zeeman splitting in terms of number of pixels is $p' = \Delta\lambda'/\Delta r'_p \sim \lambda_{\max}{}'^2/\Delta r'_p$. Then p' is $\sim n\lambda^2_{\max}/n^2\Delta r_p = \Delta\lambda/n\Delta r_p = p/n$. Thus, the maximum achievable Zeeman split magnitude in pixels is reduced by a factor of n.

The previous analysis, though, presents an intriguing possibility of going into the NIR region with medium-dispersion equipment to improve the peak resolution. With better NIR capabilities, the strong Ar I 965-nm line would provide an approximate 41% increase in $\Delta\lambda$ over the Ar I 811-nm line, and the He I 1083-nm lines would provide an approximate 135% increase over the He I 706-nm line. The bright 1083-nm triplet[41] consists of a separate 1082.91-nm line and two closely spaced lines at 1083.02 nm and 1083.03 nmnm, with an approximately 1:5:10 intensity ratio. The ≈0.12-nm separation makes this another candidate for pixel calibration and should show wide Zeeman splitting.

To test, we observed the 1083-nm line using a Princeton Instruments IsoPlane 320,[47] a 32 cm-focal-length spectrometer with a similar 1200-g/mm grating. The CCD can detect NIR light, but the $\Delta p = 20\,\mu$m pixels are 14 times larger than those in the MU1403. Figure 11 shows two peaks spaced 0.135 nm apart at $B = 0$. At $B = 1.07$ T, the two peaks are split into four approximately equally spaced peaks. The expected six peaks from the Paschen-Back effect are not fully resolved, but the spectrum still demonstrates a change due to the magnetic field. This demonstrates that a spectrometer with a smaller focal length, medium grating, and larger pixel size imaging camera can be used for Zeeman effect measurements in the NIR region.

Much higher resolution than ours can be achieved with specialized instruments such as long Ebert spectrographs or Echelle gratings in high orders. In the latter case, the spectral range will be limited but would provide an opportunity to study other systems with fine energy level structures. However, such study is beyond the scope of our work, which is focused on the B and λ^2 dependencies of the Zeeman and Paschen-Back effects, and calculating μ_B.

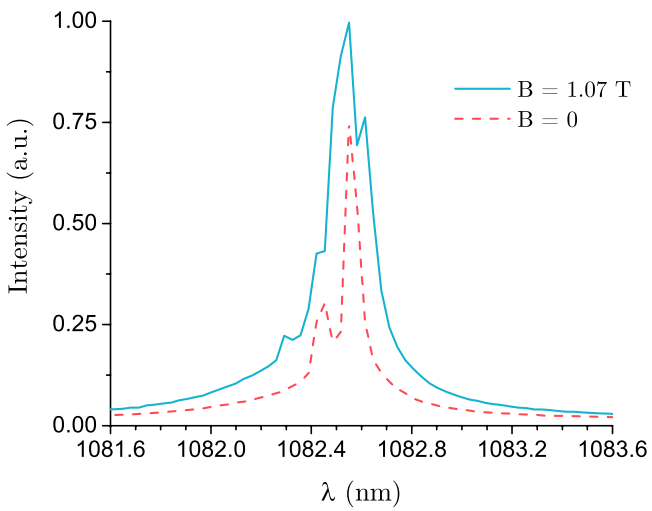

Fig. 11. Roughly calibrated He I 1083-nm line taken with the Princeton Instruments IsoPlane 320 spectrometer with $B = 1.07$ T (solid) and $B = 0$ (dashed). The He I 1082.91-nm and 1083.03-nm doublet is resolved at $B = 0$. At $B = 1.07$ T, four approximately equally spaced peaks can be distinguished. The splitting $\Delta\lambda \approx 0.12$ nm is more than twice the splitting seen in the He I 706-nm line.

VIII. CONCLUSION

We have developed an advanced laboratory experiment for studying the Zeeman and Paschen-Back effects using a 1 m Czerny-Turner spectrometer equipped with a small pixel size imaging CCD, eliminating the need for a Fabry-Perot etalon. A tunable magnet holder was built and loaded with neodymium magnets, replacing the electromagnet commonly used in these types of experiments. The use of helium and argon spectral tubes as light sources provides a dense coverage of bright lines across the VIS–NIR region. With this setup, we were able to validate that the Zeeman splitting of a line increases proportionally to the magnetic field strength. The Paschen-Back effect was demonstrated using helium lines in the VIS region. The normal and anomalous Zeeman effects were measured in Ar I lines as well.

The Bohr magneton was calculated from the measured Zeeman split in He I 447, 502, 587, 667, and 706-nm lines, and in the Ar I 811-nm line. The experimentally obtained values agree with the theoretical value within experimental error. The spectrometer has the advantage of resolving the Zeeman splitting in any detectable line in its spectral range. This provides the unique ability to investigate the λ^2 dependence, which cannot be done with a single etalon. This dependency was studied and allowed us to determine the Bohr magneton value with a second, more accurate experimental method.

Current limitations and possible improvements have been discussed. In particular, we have identified and measured the promising NIR He I 1083-nm line for demonstrating the Zeeman effect using a shorter spectrometer and common imaging camera. In summary, our new experiment can be implemented using available equipment while allowing the normal and anomalous Zeeman effects and the Paschen-Back effect to be studied in several new ways.

ACKNOWLEDGMENTS

The authors thank our colleagues Dr. Paul Champion and Dr. Mark Williams for encouragement and support of the development of this new experiment for the Advanced Physics Laboratory, and Daniel Sierpina for machining metal parts. The authors thank NEU undergraduate students Maxim Bushmelov, Matthew Fillion, Nicholas Haubrich, Christopher Moran, and Freddie Sheehan for their help in assembling the magnet holder and collecting data. The authors thank David McCrohan, of 9Scale Vacuum, for welding. The M216 spectrometer, previously used at the Harvard-Smithsonian Center for Astrophysics, is a gift from McPherson, Inc. The authors thank Dr. Erik Schoeffel of McPherson for his many insights. The authors also thank Dr. Sebastian Remi of Princeton Instruments for loaning the IsoPlane 320. The research work on high-resolution spectroscopy at the Northeastern University Plasma Laboratory was supported by AFOSR/US DOD Grants FA9550-10-1-0498 and FA2386-12-1-3006.

[1]P. Zeeman, "On the influence of magnetism on the nature of light emitted by a substance," Philos. Mag. **43**(262), 226–239 (1897).
[2]P. Zeeman, "Doublets and triplets in the spectrum produced by external magnetic forces," Philos. Mag. **44**(266), 226–239 (1897).
[3]P. Zeeman, "Doublets and triplets in the spectrum produced by external magnetic forces.-(II.)," Philos. Mag **44**(268), 255–259 (1897).

[4]H. E. White, *Introduction to Atomic Spectra* (McGraw-Hill Book Company, Inc., New York, 1934).
[5]T. Preston, "Radiation phenomena in the magnetic field," Philos. Mag. **45**(275), 325–339 (1898).
[6]F. Paschen and C. Runge, "On the radiation of mercury in the magnetic field," Astrophys. J. **15**(4), 235–251 (1902).
[7]F. Paschen and C. Runge, "On the separation of corresponding lines in the magnetic field," Astrophys. J. **16**(3), 123–134 (1902).
[8]G. E. Uhlenbeck and S. Goudsmit, "Spinning electrons and the structure of spectra," Nature **117**, 264–265 (1926).
[9]F. R. Bichowsky and H. C. Urey, "A possible explanation of the relativity doublets and anomalous Zeeman effect by means of a magnetic electron," Proc. Natl. Acad. Sci. **12**(2), 80–85 (1926).
[10]R. de L. Kronig, "Über die intensität der mehrfachlinien und ihrer Zeemankomponenten," Z. Phys. **31**, 885–897 (1925).
[11]W. Pauli, "Über den einfluss der geschwindigkeitsabhängigkeit der elektronenmasse auf den Zeemaneffekt," Z. Phys. **31**, 373–385 (1925).
[12]W. Heisenberg, "Zur quantentheorie der multiplettstruktur und der anomalen Zeemaneffekte," Z. Phys. **32**, 841–860 (1925).
[13]W. Heisenberg, "Quantentheoretische umdeutung kinematischer und mechanischer beziehungen," Z. Phys. **33**, 879–893 (1925).
[14]J. D. Hey, C. C. Chu, S. Brezinsek, Ph. Mertens, and B. Unterberg, "Oxygen ion impurity in the TEXTOR tokamak boundary plasma observed and analyzed by Zeeman spectroscopy," J. Phys. B: At. Mol. Opt. Phys. **35**, 1525–1553 (2002).
[15]K. Mizushiri *et al*., "A simultaneous measurement of polarization-resolved spectra of neutral helium 2^3P–3^3D, 2^1P–3^1D and 2^3P–3^3S emissions from the periphery of a Large Helical Device plasma," Plasma Phys. Control. Fusion **53**, 105012 (2011).
[16]T. Skikama, S. Kado, H. Zushi, A. Iwamae, and S. Tanaka, "Application of the Zeeman patterns in Ov and H α spectra to the local plasma diagnostics of the TRIAM-1M tokamak," Phys. Plasma **11**(10), 4701–4708 (2004).
[17]Ch. Uihlein and L. Eaves, "High-magnetic-field Zeeman spectroscopy of the 0.84-eV Cr-related emission and absorption line in GaAs(Cr): Experiment and theory," Phys. Rev. B **26**(8), 4473–4484 (1982).
[18]M. C. Veale *et al*., "Chromium compensated gallium arsenide detectors for X-ray and γ-ray spectroscopic imaging," Nucl. Instrum. Meth. A **752**, 6–14 (2014).
[19]D. Deming, R. J. Boyle, D. E. Jennings, and G. Wiedemann, "Solar magnetic field studies using the 12 micron emission lines. I. Quiet sun time series and sunspot slices," Astrophys. J. **333**, 978–995 (1988).
[20]H. W. Babcock, "Zeeman effect in Stellar Spectra," Astrophys. J. **105**, 105–119 (1947).
[21]R. I. Anderson, A. Reiners, and S. K. Solanki, "On detectability of Zeeman broadening in optical spectra of F- and G-dwarfs," Astron. Astrophys. **522**(A81), 1–17 (2010).
[22]J. D. Bailey, "Measuring the surface magnetic fields of magnetic stars with unresolved Zeeman splitting," Astron. Astrophys. **568**(A38), 1–6 (2014).
[23]S. V. Berdyugina and S. K. Solanki, "The molecular Zeeman effect and diagnostics of solar and stellar magnetic fields I. Theoretical spectral patterns in the Zeeman regime," Astron. Astrophys. **385**(2), 701–715 (2002).
[24]Wilton L. Virgo, "Simultaneous Stark and Zeeman effects in atoms with hyperfine structure," Am. J. Phys. **81**(12), 936–942 (2013).
[25]S. George, "Normal and anomalous Zeeman effect laboratory experiments," Am. J. Phys. **41**, 423–425 (1973).
[26]C. L. Schreiber, Eugene Y. Wong, and David Johnston. "Low-cost, high-resolution ebert spectrograph for a teaching laboratory," Am. J. Phys. **39**, 1333–1336 (1971).
[27]Adrian C. Melissinos, *Experiments in Modern Physics*, 1st ed. (Academic Press, Boston, MA, 1966), pp. 280–327.
[28]Daryl W. Preston and Eric R. Dietz, *The Art of Experimental Physics* (John Wiley & Sons, New York, NY, 1991), pp. 241–263.
[29]Jennifer Blue, S. Burcin Bayram, and S. Douglas Marcum, "Creating, implementing, and sustaining an advanced optical spectroscopy laboratory course," Am. J. Phys. **78**(5), 503–509 (2010).
[30]Complete Zeeman effect Apparatus from Spectrum Scientifics, <http://www.spectrum-scientifics.com/Complete-Zeeman-effect-Apparatus-p/2483.htm>.
[31]Junior Lab, course 8.13, lab number 6 at Massachusetts Institute of Technology, <http://web.mit.edu/8.13/www/06.shtml>.
[32]K. A. Pietraszewski and A. G. Meldrum, "Cryogenic servo-stabilized Fabry-Perot interferometer for imaging at 2-2.5 microns," Proc. SPIE **2814**, 139–146 (1996).
[33]O. Batishchev, "Minihelicon plasma thruster," IEEE Trans. Plasma Sci. **37**(8), 1563–1571 (2009).
[34]O. Batishchev and J. L. Cambier, "Experimental study of the mini-helicon thruster," Air Force Research Laboratory Report, AFRL-RZ-ED-TR-2009-0020 (2009).
[35]Pasco Scientific Spectral Tube Power Supply and Mount, <http://www.pasco.com/prodCatalog/SE/SE-9460_spectral-tube-power-supply-and-mount>.
[36]Permanent magnets purchased from Applied Magnetics, <http://www.magnet4less.com/index.php?cPath=1_11>.
[37]The currently available McPherson 2061 has similar performance to the M216, <http://mcphersoninc.com/spectrometers/uvvisir/model2061.html>.
[38]14MP USB3.0 Real-Time Live Video Microscope USB Digital Camera, <http://www.amscope.com/14mp-usb3-0-real-time-live-video-microscope-digital-camera-10-mp.html>.
[39]Ocean Optics - USB4000-UV-VIS, <https://oceanoptics.com/product/usb4000-uv-vis/>.
[40]SpectraSuite software bundled with the USB4000 spectrometer has been discontinued and replaced with OceanView; <https://oceanoptics.com/product/oceanview/>.
[41]NIST Atomic Data for Helium, <http://www.physics.nist.gov/PhysRefData/Handbook/Tables/heliumtable1.htm>.
[42]NIST Atomic Data for Argon, <http://www.physics.nist.gov/PhysRefData/Handbook/Tables/argontable1.htm>.
[43]F. Paschen and E. Back, "Liniengruppen magnetisch vervollständigt," Physica **1**, 261–273 (1921); available at https://babel.hathitrust.org/cgi/pt?id=mdp.39015009233449;view=1up;seq=7.
[44]H. Odenthal, R. Rambau, E. K. Souw, and J. Uhlenbusch, "The Zeeman splitting of the 5876 Å helium line studied by means of a tunable dye laser," Physica B+C **113C**(2), 203–216 (1982).
[45]Northeastern University Introductory Physics Laboratory Straight-Line Fit Calculator, <http://www.northeastern.edu/ipl/data-analysis/straight-line-fit/>.
[46]J. B. Green and B. Fried, "The Zeeman effect in the spectrum of argon," Phys. Rev. **54**, 876–882 (1938).
[47]Princeton Instruments—IsoPlane aberration-reduced spectrographs, <http://www.princetoninstruments.com/products/spec/isoplane/>.